

# Optical Engineering

[OpticalEngineering.SPIEDigitalLibrary.org](http://OpticalEngineering.SPIEDigitalLibrary.org)

## **Dragonfly directional sensor versus rocket-propelled grenades**

Joseph Geary  
Lisa Blackwell

# Dragonfly directional sensor versus rocket-propelled grenades

Joseph Geary\* and Lisa Blackwell

University of Alabama Huntsville, Center for Applied Optics, 301 Sparkman Drive, Huntsville, Alabama 35899, United States

**Abstract.** The Dragonfly directional sensor was deployed at the Army's Yuma Proving Grounds for preliminary field tests against rocket-propelled grenades. This wide-field (nonimaging) sensor's purpose was to angularly locate the latter's launch plume. These tests successfully demonstrated proof-of-concept. © The Authors. Published by SPIE under a Creative Commons Attribution 3.0 Unported License. Distribution or reproduction of this work in whole or in part requires full attribution of the original publication, including its DOI. [DOI: [10.1117/1.OE.54.2.025115](https://doi.org/10.1117/1.OE.54.2.025115)]

Keywords: Dragonfly; coherent fiber arrays; directional sensing.

Paper 141473 received Sep. 18, 2014; accepted for publication Jan. 27, 2015; published online Feb. 24, 2015.

## 1 Introduction

This is a sequel to our Dragonfly paper published in February 2013.<sup>1</sup> That paper concentrated on laboratory tests whose purpose was the characterization and calibration of the Dragonfly optic<sup>2</sup> and its incorporation into a laboratory version of a Dragonfly directional sensor (DDS). The DDS is a very wide-field nonimaging sensor which has the capability to locate and track multiple bright objects against a darker background. The DDS has many potential application areas. One such area of particular concern for the Army is the detection of rocket-propelled grenade (RPG) launch points. RPGs are a pernicious problem in tactical environments. The RPG is a man portable, short-range weapon with a powerful punch. The most notable feature is their bright launch plume, which persists for ~10 ms. Consequently, timely detection of the launch flash is a critical component to any RPG negation system. Optical systems have shown promise in this regard. Relevant systems can be found in the patent literature. Patents U.S.7492308 and U.S.8526671 provide two such examples.<sup>3,4</sup> The first incorporates a panoramic imaging system consisting of two imaging arrays and three cameras (from O.D.F Optronics Ltd.). The second utilizes a fairly complex panoramic imaging system to accomplish its goals.

A test of opportunity for the DDS presented itself at the Army's Yuma Proving Grounds (YPG). A field DDS prototype was quickly built in order to piggy-back on the already scheduled test series. Our primary purpose was demonstrating DDS proof-of-concept in a real-world environment. This paper discusses the predeployment calibrations, the data collected during deployment, and the post-test analysis of that data (including a range determination protocol).

## 2 DDS Structure

The heart of the DDS is the Dragonfly optic shown in Fig. 1. It is a coherent rectilinear array of approximately three million fused optical fibers (core and cladding). The key design feature is that individual fibers must be perpendicular to both the convex input surface and also the flat output surface, which is then coupled to a focal plane array. Thus, the natural

coordinate system of the Dragonfly optic is polar. It is this unique design that makes the DDS a wide-field directional tracking sensor that connects a certain pixel to a specific elevation and azimuth angle. (Note: Detailed information about Dragonfly characteristics can be found in Ref. 1.)

The internal arrangement of a basic DDS is displayed in Fig. 2(a). On the right is the Dragonfly optic. This is followed by an interference filter, a relay lens, and, finally, a digital CCD. A major chemical component in the launch flash is potassium. It has a very strong spectral signature at  $\lambda = 770$  nm, hence the interference filter for this wavelength. This filter also greatly reduced ambient background light since the YPG tests were conducted in bright sunlight. The digital CCD was run at 150 frames per second (or 6.7 ms per frame). In operation, a distant external bright source will show up as a hot spot on the flat side of the Dragonfly optic. This hot spot is then imaged onto the CCD by the relay optic. The hot spot's centroid identifies the elevation and azimuth angle of the external source, which, in this case, is the RPG launch plume. (Note: Our lab DDS was able to locate the hot spot centroid to a tenth of a degree.) The DDS package is fairly compact and weighs 1 lb.

Power for the EPIX digital CCD was provided by a PC collocated with the DDS. This PC also supported the operational software that came with the CCD. Because of safety issues, operation of the DDS/PC was done remotely via a laptop located up-range and connected via a wireless hookup. Software written in LabView for the laptop provided the operator with direct control over the down-range DDS/PC. A block diagram of the overall system arrangement is portrayed in Fig. 2(b).

## 3 DDS Calibrations Prior to Deployment

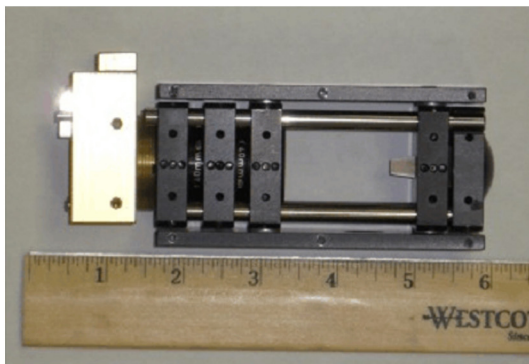
### 3.1 Radiometric Calibration

The Dragonfly system obtains irradiance data indirectly in terms of counts. These counts need to be connected to a physically meaningful value, such as W/cm<sup>2</sup>. This was accomplished in our UAH lab in the following manner. In Fig. 3, we have the DDS system (left) coaligned to a collimator (right). The collimated light power level is adjustable and we used several different settings. The DDS count level for each setting is recorded. In Fig. 4, a radiometer (center) is

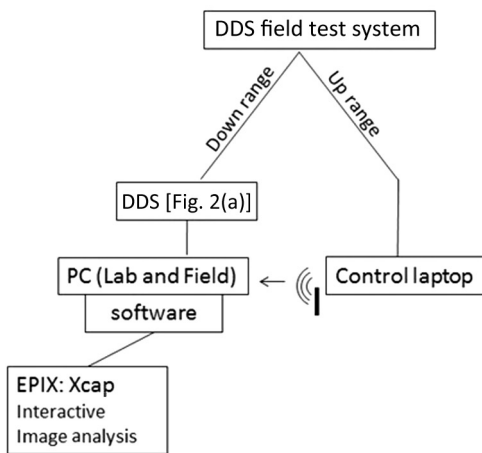
\*Address all correspondence to: Joseph Geary, E-mail: [gearyj@uah.edu](mailto:gearyj@uah.edu)



**Fig. 1** Dragonfly optic (prototype #2) mounted in a 40 mm square frame.



(a)



(b)

**Fig. 2** (a) The Dragonfly directional sensor (DDS) system used at Yuma: right to left are the Dragonfly optic, an interference filter, a relay lens, and the digital CCD. (b) Block diagram of field test system.

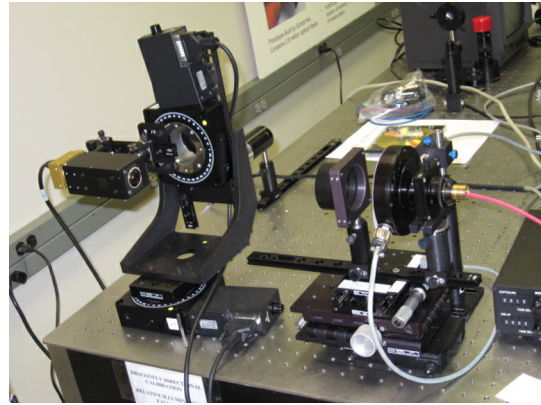


**Fig. 3** DDS measurement in counts.

interposed between the DDS and the collimated beam. The radiometer is aligned to the collimated beam and its aperture is masked to the same size as the Dragonfly aperture.

The collimated beam irradiance is uniform, but it is important that the beam overfills both the detector aperture and the Dragonfly aperture. For each previous setting of the collimated beam, the radiometer reads the light level in terms of  $W/cm^2$ .

The purpose here is to directly tie the DDS signal in counts to the corresponding radiometer irradiance signal measured in  $W/cm^2$  using the same source. Note that both instruments incorporate a potassium isolating interference filter at  $\lambda = 770$  nm. A uniform collimated beam incident on the spherical side is converted to a nonuniform but rotationally symmetric hot spot on the flat side. The relay lens images that hot spot onto the CCD array after the focused beam passes through the 770 nm interference filter. Figure 5 shows the DDS response for an irradiance level at its entrance aperture. What you see on the top block is the hot spot image on the CCD. Note the dashed horizontal line passing through the center of the hot spot. This horizontal line defines a row of pixels. The irradiance level on each pixel is read out in counts (on the left hand y-coordinate axis). This profile is displayed in the lower block. The peak of the profile is at the center of the hot spot. We measure the height of that peak in counts relative to the background base (sitting at 132 counts). Next, we relate that peak to the

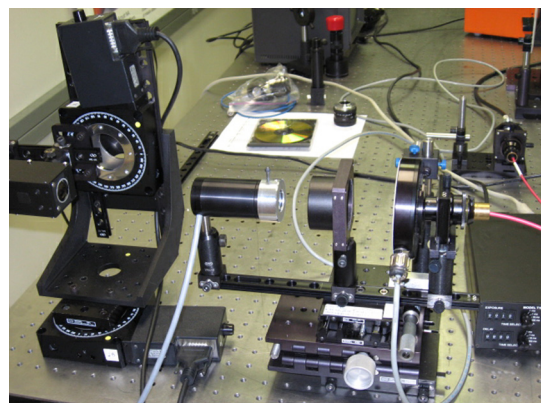


**Fig. 4** Radiometer measurement in  $W/cm^2$ .

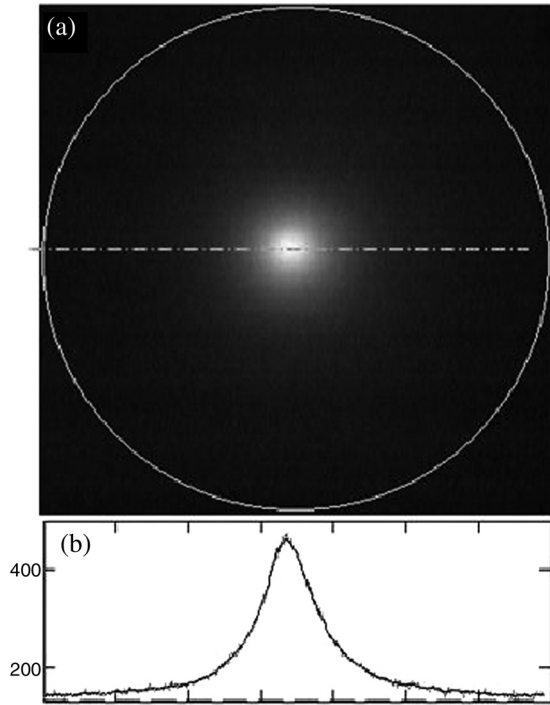


**Fig. 5** DDS response to an irradiance level at its entrance aperture. (a) Image of hot spot. The white outer ring denotes the boundary of the flat output side. (b) Count profile through the center of the hot spot.

actual irradiance level at the entrance aperture. Four different irradiance levels were utilized.

Figure 6 enlarges and overlaps all the profiles from all four irradiance levels utilized in this calibration. The noisy profiles are first fitted with a smooth curve. Peak values both in counts and in terms of the irradiance at the Dragonfly entrance aperture are shown. Table 1 correlates peak counts (minus the base) with the irradiance present at the entrance aperture. Table 1 is plotted in Fig. 7.

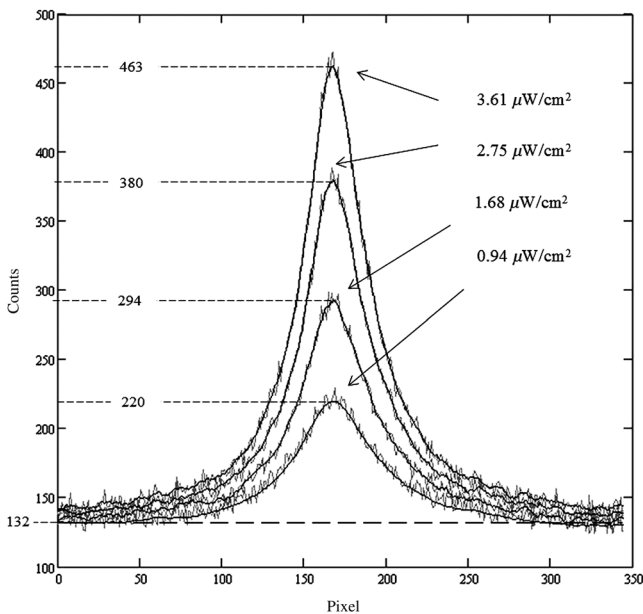


**Fig. 6** Hot spot profiles for four irradiance levels at the entrance aperture.

**Table 1** Irradiance related to counts at Dragonfly directional sensor (DDS) entrance aperture.

Entrance aperture irradiance ( $\mu\text{W}/\text{cm}^2$ )	Peak count level minus base
3.61	331
2.75	248
1.68	162
0.94	88

The highest irradiance that our lab collimated beam could achieve was at the fourth point on the chart. But we suspected that the RPG flash would likely be much higher. Also, the measured irradiance would depend on the DDS location relative to the launch point (which was not known ahead of time). Since both the radiometer and the DDS are linear detectors, we extrapolated the plot out to 900 counts (which was the current limit imposed by the DDS software). Then 900 counts will correspond to  $9.97 \mu\text{W}/\text{cm}^2$  at the DDS entrance aperture.

**3.2 Relative Illumination Falloff Calibration**

Relative illumination falloff (RIF) is a measurement term originally used in the context of photographic imaging lenses. Basically, it means that the irradiance at any given field position in the image is a function of the field angle given the same incident irradiance on a system’s entrance pupil. The irradiance is normally highest on-axis but falls off with increasing field angle. The RIF measurement for the Dragonfly optic (Fig. 1) was presented in Ref. 1, and

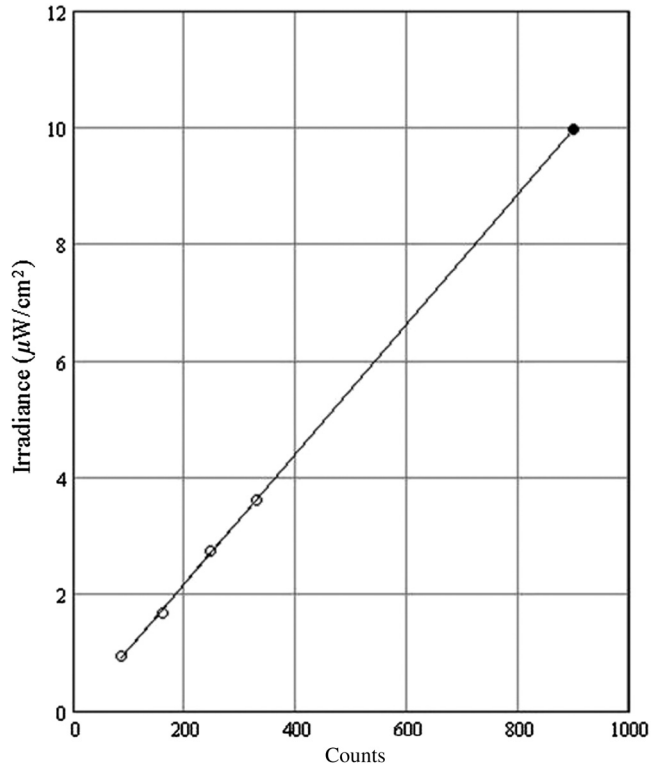


**Fig. 7** Plot of Table 1 connecting Dragonfly counts to  $\mu\text{W}/\text{cm}^2$ .

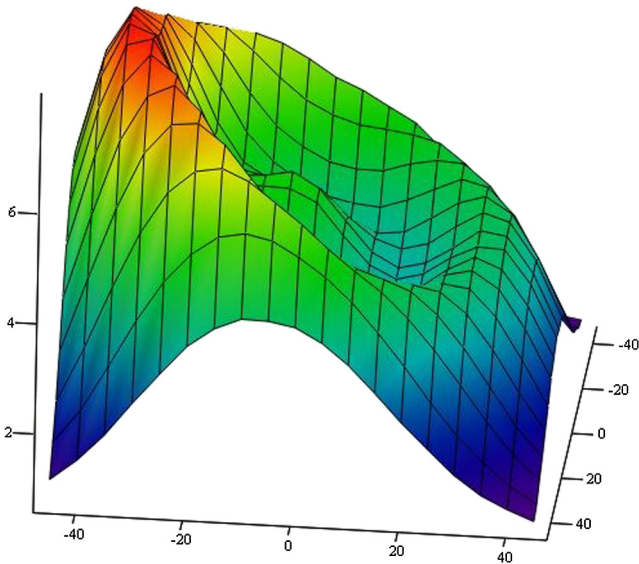


**Fig. 8** Relative illumination falloff (RIF) test on Dragonfly optic prototype #2.

is reproduced here as Fig. 8. For this measurement, the output side of the Dragonfly optic was directly coupled into an integrating sphere because the numerical aperture is approximately one on the flat side. This was necessary integrating sphere because the numerical aperture is approximately one on the flat side. Ideally, the RIF plot should be rotationally symmetric, but in Fig. 8, it is not. The plot exhibits strong and asymmetric RIF characteristics, which complicates the radiometric response. (Note: Symmetric RIFs are expected as the fabrication process improves.)

For CCD cameras with pixels having identical characteristic curves but located at different field positions, the pixel response is tied to the local irradiance at that location. Consequently, we need the RIF response for the DDS system. (Note: RIF information is embedded in the azimuth/elevation calibration data that made use of the test setup shown in Fig. 3 but where the dual orthogonal rotation stages were exercised through their respective angles). To extract

RIF, the following procedure was used for each measurement angle. First, a threshold on the hot spot counts was set at 90%, i.e., all counts <90% were ignored. Second, all the pixel counts sitting above the threshold were added up. Third, those counts were divided by the number of pixels sitting at the threshold (thus getting the average counts per pixel). The third step was needed to account for the change in size and shape of the hot spot as a function of angle. The hot spot is small and round in the center, but gets bigger and elongates especially near the edge. The resultant RIF plot using this approach is shown in Fig. 9 (crosshairs mark  $\pm 45$  deg).

#### 4 DDS Yuma Test

##### 4.1 On-Site Test Geometry

The geometric relationship among the launch point, DDS, and target location is shown in Fig. 10. The DDS optical axis was pointed across the RPG track such that both the launch position and target were well within its full field of view (FFOV) of 90 deg. From Fig. 10, we see that the

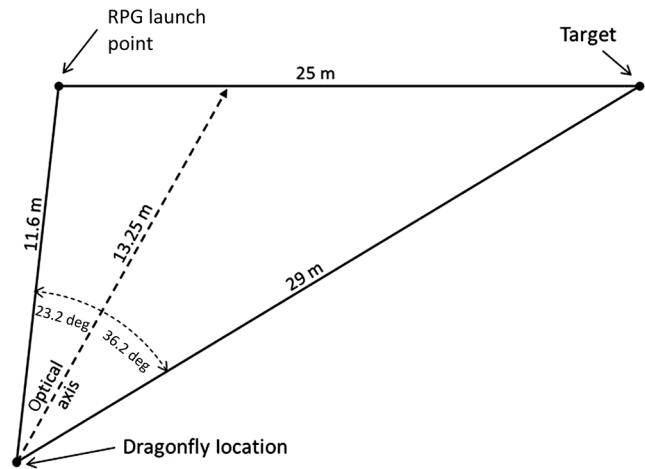


**Fig. 10** Test geometry for rocket-propelled grenade (RPG) shots showing the location of the DDS relative to the launch point and war-head detonation at the target.

#### Calculated RIF using only the hotspot

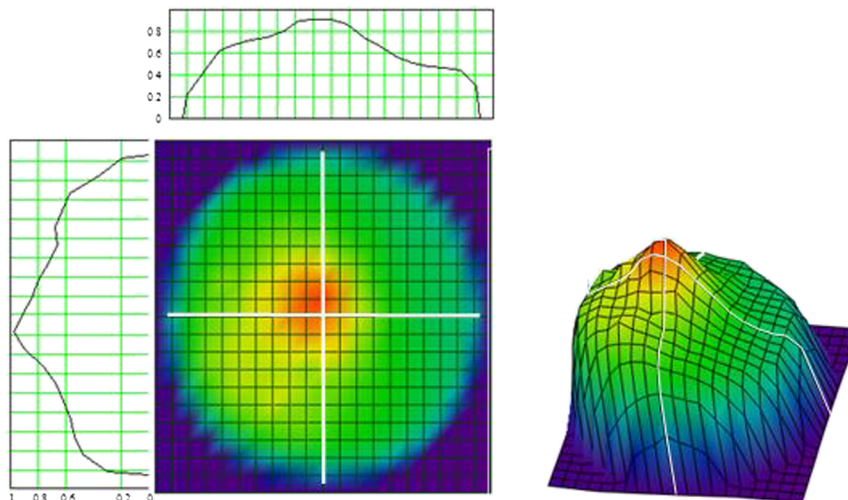


**Fig. 9** RIF plots (two-dimensional and three-dimensional) and profiles for DDS system used at Yuma.

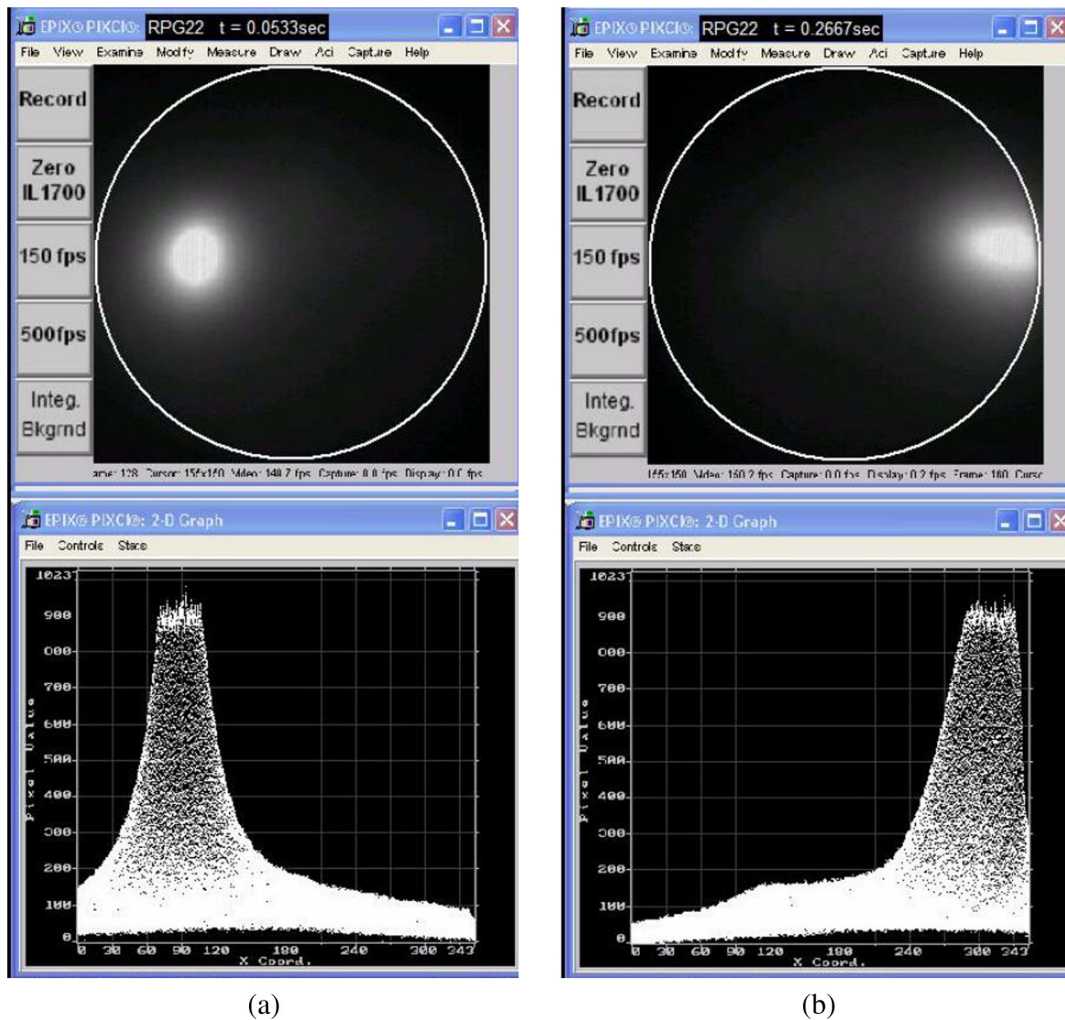


Fig. 11 RPG#22 as viewed by the DDS: (a) launch and (b) detonation on target.

full angle between the launch and target was 59.4 deg, which fit comfortably within the DDS FFOV. The launch to target distance was 25 m. At this short range, things happen very quickly. (For example, the sound of the launch and detonation seemed almost simultaneous.) There was a countdown provided over a loud speaker, which became silent when it passed 6 s. Thereafter, the operator had to continue the count mentally (which sometimes led to missing a launch altogether).

**4.2 DDS Data Collection**

One surprise on-site for us novices was the presence of a strong potassium signal in the detonation flash at the target. This was a bonus signal, which helped establish a track (as there was no apparent signal from the rocket exhaust). For our purposes, here we will concentrate our attention on RPG#21 and 22 for which both launch and detonation data were obtained. We start by looking at the initial data for RPG#22 as shown in Fig. 11.

Images of the Dragonfly optic flat face are shown at the top of Fig. 11. Profiles are shown directly underneath. It is important to note that these profiles are summations of total column counts as a function of  $x$ . This was a useful feature option on-site because it provided the operator with

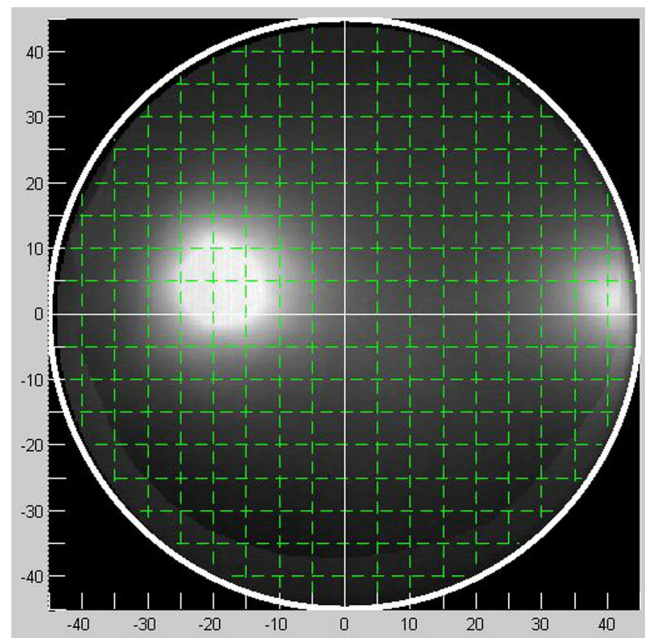
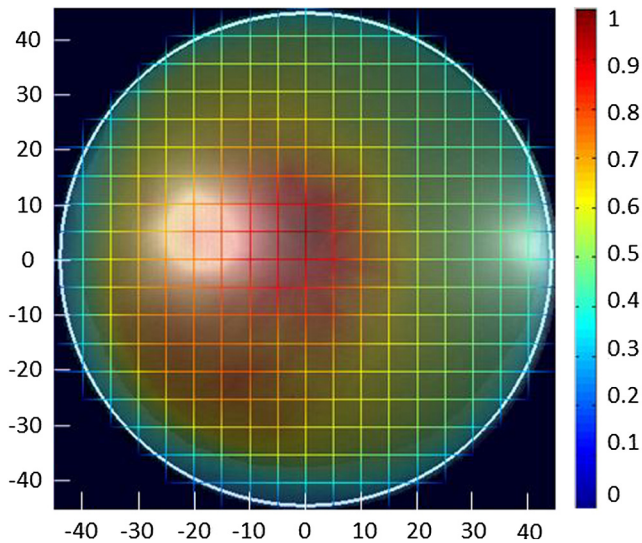


Fig. 12 Reprise of Fig. 11 but now on a common display and calibrated in terms of azimuth/elevation angle.



**Fig. 13** RIF plot from Fig. 9 overlaid on DDS plot for RPG#22 as shown in Fig. 12.

eye-catching visual proof that the DDS saw both the launch and detonation. The flight time between launch and detonation is 0.2134 s. The angular separation is  $\sim 60$  deg. The digital camera exposure time was set for 1.5 ms.

As already mentioned, the natural coordinate system for the Dragonfly optic is polar. However, what is shown in Fig. 12 is a post-test reinterpretation of RPG#22 data from Fig. 11 in a rectilinear angular format. Here both launch and detonation are shown on the same display even though they occurred at different times. The respective hot spot (centroid) locations can be read directly from this display at their proper azimuth and elevation angles. The launch plume is located at  $(-17.5$  deg,  $+5$  deg). The detonation is located at  $(+40$  deg,  $+2.5$  deg).

We now fold into Fig. 12 the results of the RIF data from Fig. 9. The overlaid plots are shown in Fig. 13. Knowing

what the RIF impact is allows one to determine the input signal strength when the DDS is at an angle relative to the launch point (Fig. 10).

## 5 Post-Test Radiometric Analysis of Launch Plume Data

From the calibrated azimuth/elevation pixel position data in Fig. 12 coupled with the overlaying RIF data (Fig. 13), we are now able to extract the radiometric information for the RPG#21 and 22 launch plumes.

### 5.1 First Order

Now that we have a reasonable connection between Dragonfly counts and radiometric values in  $W/cm^2$ . (via Fig. 7), we can apply this to the launch plume data. The launch plume images and profiles for RPG#21 and 22 are shown in Figs. 14(a) and 14(b). As you can see, RPG#22 is saturated, while RPG#21 is not. We believe this to be simply a matter of luck. Recall that the CCD camera frame rate was 150 fps, which means a frame time of 6.7 ms. This combined with the manual nature of the countdown resulted in a trigger occurring either too early or too late to catch the full peak of the launch plume. The peak for RPG#21 sits at approximately at 1023 counts (neglecting background). Using the data plotted in Fig. 7 (and assuming linearity), those counts correspond to  $11.33 \mu W/cm^2$  at the Dragonfly entrance aperture. However, we still have to make a correction to account for the angle of the launch plume relative to the pointing direction of Dragonfly (Fig. 10). Relative illumination falloff (Sec. 3.2) comes into play here. This means that the actual  $\mu W/cm^2$  impinging on the Dragonfly aperture at this viewing angle of 23.3 deg will be larger.

For example, at the peak pixel location in Fig. 14(a) for RPG#21, the RIF value (based on Fig. 13) is 78.6% or 0.786. Therefore, the corrected irradiance value is:

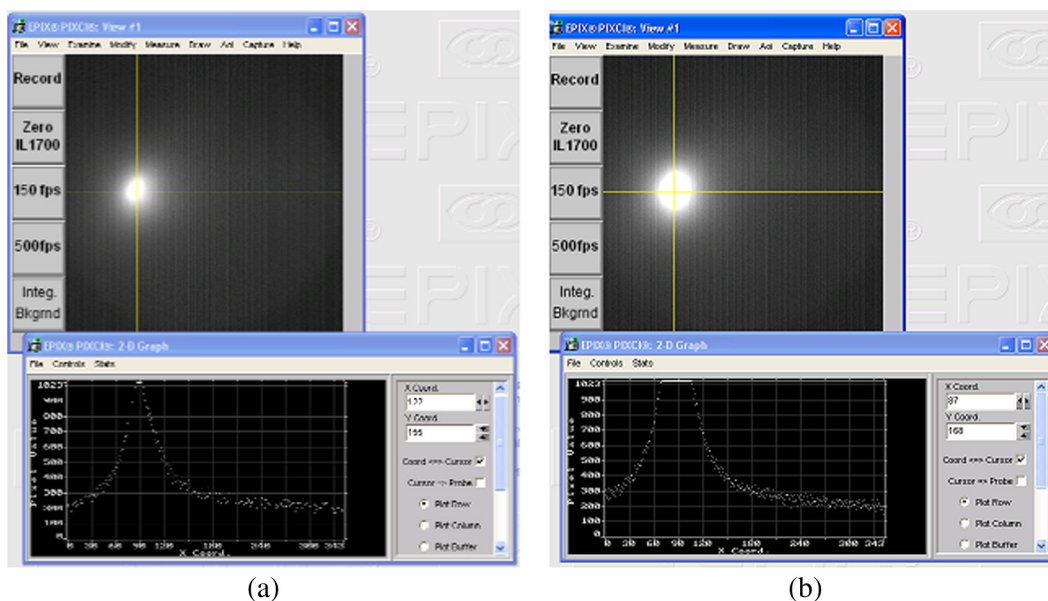


**Fig. 14** DDS launch plume image (top) and row profile (bottom) for (a) RPG#21 and (b) RPG#22. (Note: The x-axis profiles shown below each image are for a row of pixels along the horizontal line. They are not column summations as previously used in Fig. 11.)

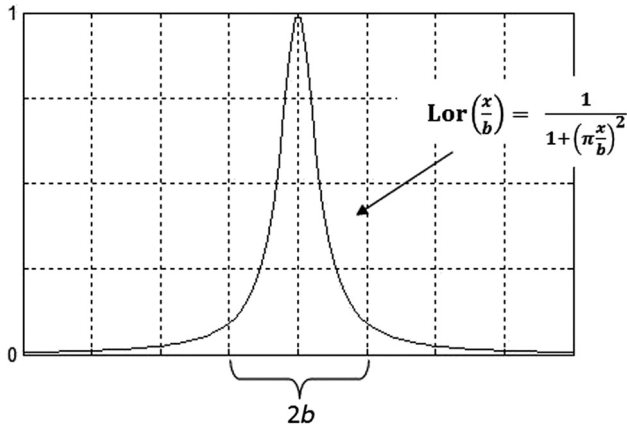


Fig. 15 The Lorentzian profile and equation.

$$I_{cor} = I_{meas} \div RIF = 11.33 \mu\text{W}/\text{cm}^2 \div 0.786 = 14.41 \mu\text{W}/\text{cm}^2.$$

5.2 Lorentzian Data Fit Analysis

We can take this preliminary analysis one step further. The launch profile in Fig. 14(a) resembles the mathematical profile known as a Lorentzian. This profile is shown in Fig. 15 (with the descriptive equation on the right).

The idea is to fit the launch profile in Fig. 14(a) to a Lorentzian to see how well they match. If the match is reasonable, we then turn our attention to the launch profile in Fig. 14(b). We assume that its generic curve is also Lorentzian. Even though its profile is saturated, we can fit the data we do have to a Lorentzian and thereby extrapolate the location of its peak in counts. We then relate that value to  $\mu\text{W}/\text{cm}^2$ . However, in order to properly fit a Lorentzian to the launch profile for RPG#21 and 22, the background counts have to be removed first. The fit results are shown in Figs. 16(a) and 16(b). In each figure, two plots are shown. The bottom curve is the background corrected plot. The top curve is the Lorentzian fit. Once done, we now see

that the data profile in Fig. 16(a) plateaus out around 846 counts, thus indicating some signal saturation. However, the Lorentzian fit extrapolates beyond this to a sharp peak at 1050 counts, or  $11.63 \mu\text{W}/\text{cm}^2$  (via Fig. 7). This irradiance still needs to be corrected for RIF, which leads to  $I_{cor} = 14.8 \mu\text{W}/\text{cm}^2$ .

In Fig. 16(b), the data plot for RPG#22 (with background removed) plateaus out around 846 counts as well. The Lorentzian fit extrapolates this to a peak at 1450 counts, or  $16.06 \mu\text{W}/\text{cm}^2$  (via Fig. 7). Taking RIF into account results in  $I_{cor} = 20.4 \mu\text{W}/\text{cm}^2$ .

The Lorentz fitting has provided a reasonable value for the irradiance peak at the center of the hot spot for RPG#21 and RPG#22, respectively. However, we also know that we caught RPG#22 at a better temporal slice. But we have no guarantee that the peak in this slice represents the highest. This is due to a combination of triggering issues, and just where the 1.5 ms exposure was made during the evolution of the flash. We examine this issue in the next section.

5.3 Triggering Versus Frame Rate and Exposure Time

As already mentioned, a single frame lasts 6.7 ms, but the exposure time within that frame was set at 1.5 ms. This is illustrated in Fig. 17(a). Note the dead time within each frame of 5.2 ms. No data can be collected here. In Figs. 17(b)–17(e), the RPG flash event (and duration) is represented by a blue (isosceles) triangle. In Fig. 17(b), the only portion of the event is that captured within the exposure window. The rest of the event lies in the dead time. If the launch plume flash lasts  $>6.7$  ms, portions of it will show up in two successive frames as in Fig. 17(c). We have not seen this in the data, which leads us to conclude that the plume flash lasts 5.2 ms or less. If the flash is coincident with the frame’s dead time, it will not be seen at all even though it lies within the overall frame time as in Fig. 17(d). The most significant signal should occur when the exposure window is centered on the flash peak as in Fig. 17(e). (But that would require serendipitous manual triggering.)

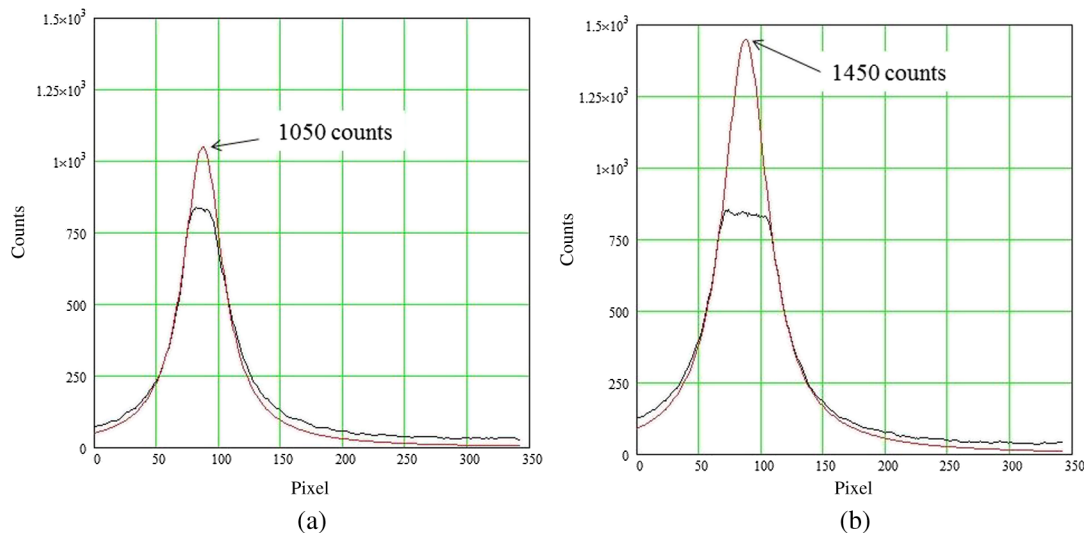
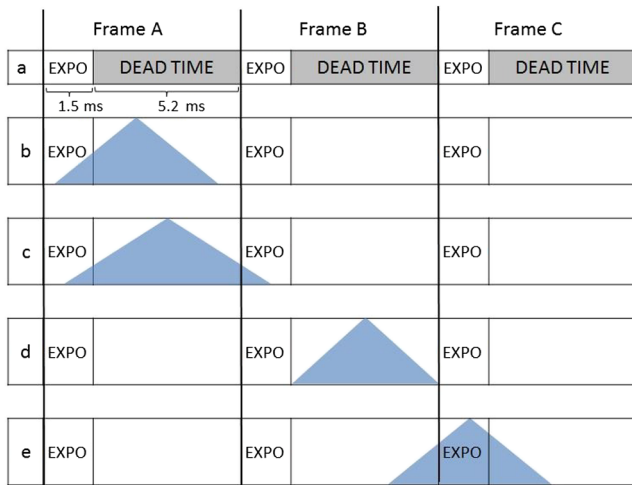


Fig. 16 Lorentzian fits (top curves) to launch profiles (bottom curves) for (a) RPG#21 and (b) RPG#22 (The bottom curves are for background corrected data).



**Fig. 17** Frame time versus exposure time versus RPG relative flash locations and duration: [parts (a) to (e)].

From Fig. 17, there is now an upper boundary on a launch flash duration of ~5 ms (and not the 10 ms we were initially told). For the digital camera used at Yuma, the exposure time can be adjusted up to a max value of 6.7 ms. The lesson learned for future RPG testing with the DDS is to set the camera exposure time to at least 5 ms. But triggering with the silent count still remains problematic.

### 6 Range to Launch Point

The DDS provides a direction in terms of azimuth and elevation of a bright source against a darker background. But unless you know *a priori* the properties of that bright source (e.g., RPG launch plume radiance), it will be difficult to determine an accurate range from DDS data. At Yuma, the launch signals seen by DDS were mostly saturated because we were too close to the launch plume. Only through the analysis in Sec. 5 were we able to determine the approximate irradiance at the DDS aperture itself. You would also want to know (given an RPG launch) how far away from the launch plume can you be before the DDS signal is buried in the noise? But the piggyback testing at Yuma was not configured to answer that particular question. However, if you have two DDS systems working in concert, you can determine the range using triangulation. This is shown conceptually in Fig. 18.

In Fig. 18(a), both DDS systems have to be aligned (optical axes parallel) and laterally separated by a known amount. Each DDS will provide a direction angle to the distant source. Lines drawn along those direction angles will cross at the source. Now we have a triangle set with known angles and a base separation. Triangulation can now be used to angularly locate that source relative to the DDS pairs' location. Figure 18(b) shows a setup that can be employed in the limited confines of a laboratory to simulate triangulation. Here a collimator is used at two different rotation angles. Each DDS views the collimated beam when it is pointed at them. Each DDS then reports an arrival angle for the collimated beam. Here the angles as determined by each DDS supply the critical information for triangulation. Unfortunately, the lab setup in Fig. 18(b) will have to be modified further because, in reality, we only have one

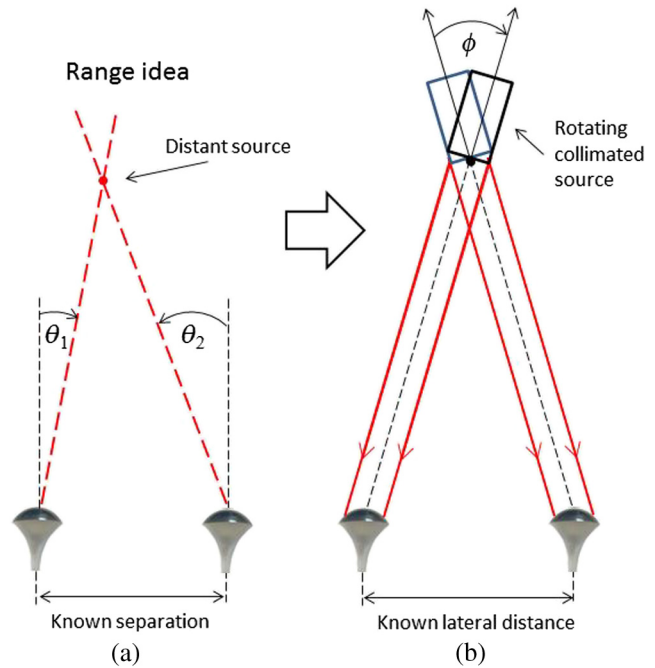


**Fig. 18** Conceptual scheme for determining range via triangulation: (a) finite distant source and (b) lab simulation using a collimator (here angles provide the critical information).

DDS system available. Consequently, that DDS will have to be used sequentially at two laterally separated locations. This is shown in Figs. 19(a) and 19(b), where a collimator mounted on a rotation stage is used to point a collimated beam at the DDS after the latter has been shifted to two different lateral locations.

The collimator is at the top of photos in Figs. 19(a) and 19(b). The geographic position of the collimator is fixed but its azimuth angle is not. The rotation stage axis passes through the front vertex of the collimating lens. The DDS system is at the bottom of the photos in Figs. 19(a) and

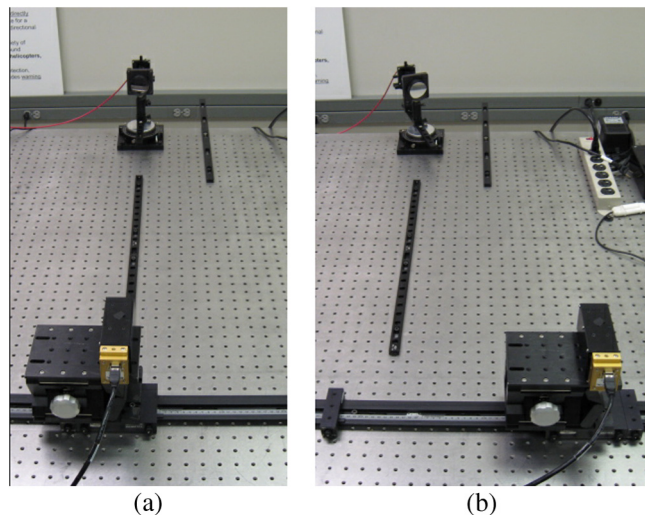


**Fig. 19** (a) Collimator and DDS axes are aligned (rotation stage reads 0 deg). (b) Collimator is rotated to 20 deg and DDS shifted laterally to recenter on collimated beam.

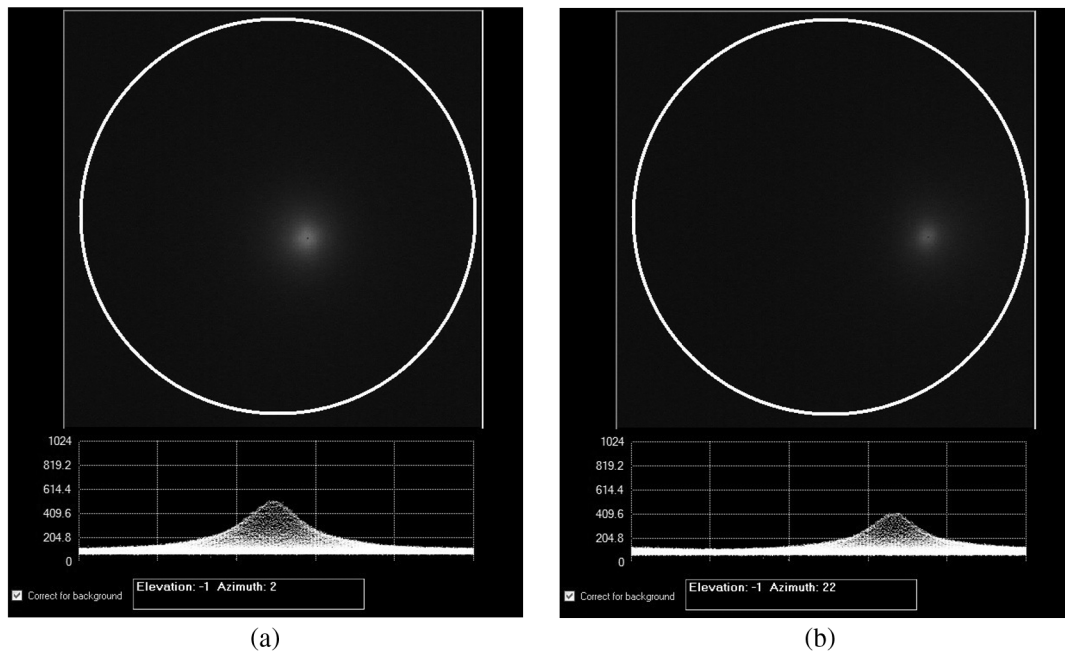


Fig. 20 Data display for (a) 0 deg and (b) 20 deg.

19(b). The DDS sits atop an elevation stage/carriage/rail system. The DDS can be positioned laterally anywhere along the rail, but at least two positions are needed to represent two DDS systems working in concert (but its optical axis is always pointing normal to the lateral separation line). The collimator's beam will point angularly toward, be centered on, and overflow the DDS apertures at both locations. Please note that since we are working at finite distances using collimated light, our main interest here is not range per se but rather the pair of direction angles supplied by the DDS at each location. Those angles have to match the readings on the rotation stage supporting the collimator.

Figures 20(a) and 20(b) show the DDS displays for the two data sets acquired. Note the lateral shift between them. Also note the lower irradiance in Fig. 20(b) compared to Fig. 20(a). This is due to relative illumination effects (Sec. 3.2). New software was written so that the azimuth/elevation angle of the hot spot centroid (red dot) could be read directly from the data display (shown in the box below the profiles).

From Fig. 20, we can read off the hot spot centroid. For Fig. 20(a),  $EL = -1$  deg and  $AZ = 2$  deg. For Fig. 20(b),  $EL = -1$  deg and  $AZ = 22$  deg. The azimuth difference between Fig. 20(a) and 20(b) is 20 deg, which is exactly the change introduced by the rotation stage. However, there is a 2 deg bias in the centroid readings obtained by DDS. We believe this bias is attributable to some misalignment between the collimator and Dragonfly as a consequence of the two distinct setups used for angular calibration versus that used for triangulation. Also, keep in mind that in this lab demonstration, the lateral offset between Dragonfly locations was not actually utilized. Since collimated light was being used, we were not after range as such but only angles. However, in the field, lateral separation (along with Dragonfly determined angles) would most definitely be used for determining the range to the launch plume.

## 7 Discussion

As reported in this paper, a prototype DDS was taken from the laboratory environment and placed in a real-world application area, detecting an RPG launch point. We discussed the general structure of the DDS, pre-test calibrations, on-site test geometry and data collection, and post-test analysis. The latter also included how the DDS could be used for determining the range to a target. As a proof-of-concept demonstration of the DDS, this field test was successful. We believe the DDS has earned its first merit badge and is poised for the next logical step—the design, construction, and calibration of a ruggedized military sensor for use on the battle field whether that be on the ground, or airborne (as on a helicopter). Looking further into the future, we envision a more compact DDS with a wider FOV than the prototype Dragonfly optic used here. For example, imagine a CCD chip directly attached to the flat side of the Dragonfly optic. Such a small lightweight DDS might even be used onboard a missile as a solid-state seeker head, replacing the complex gimbal systems currently in use.

## Acknowledgments

This work could not have been done without the direct funding support provided by the Office of the Vice-President of Research at the University of Alabama Huntsville. Our thanks to the Army for the invitation to participate in the rocket-propelled grenade testing at Yuma Proving Grounds.

## References

1. J. Geary et al., "Dragonfly directional sensor," *Opt. Eng.* **52**(2), 024403 (2013).
2. "Fiber optic directional sensor & method," U.S. Patent No. 8,817,271 (2014).
3. Y. Benayahu and A. Voskoboinik, "Threat detection system," U.S. Patent No. 7,492,308 (2008).
4. M. Warren, M. Amon, and R. Sandh Jr., "Low cost threat detection sensor," U.S. Patent No. 8,526,671 (2009).

**Joseph Geary** received his BA in physics from LaSalle College in 1966. He received his MS and PhD in optics from the University of Arizona's Optical Sciences Center in 1975 and 1984, respectively. He has 47 years of broad-based experience in optics. He has been with the Center for Applied Optics at UA Huntsville since 1996, where he is a research professor. He has authored 44 papers in refereed journals, written four books, and holds 11 patents.

**Lisa Blackwell** received her BA in physics from Auburn University in 1994. She started her graduate work in 1996 at CREOL at the University of Central Florida. In 1997, she transferred to UA Huntsville and received her PhD in optical science & engineering in 2001. Immediately following, she joined the staff of the Center for Applied Optics as a research scientist. At the CAO, she has performed work in a wide variety of areas in optics, including design, analysis, and optical testing.